JOC Featured Article

pubs.acs.org/joc

Gas-Phase Facial Diastereoselectivity of Equatorial and Axial 4-Chloro-adamant-2-yl Cations[||]

Caterina Fraschetti,[†] Francesca R. Novara,[†] Antonello Filippi,*[,†] Maurizio Speranza,[†] Neil A. Trout,[‡] William Adcock,[‡] Enrico Marcantoni,[§] Gabriele Renzi,[§] Graziella Roselli,[§] and Mauro Marcolini[§]

[†]*Dipartimento di Chimica e Tecnologie del Farmaco, Università di Roma "La Sapienza", P.le A. Moro, 5, Roma 00185, Italy,* [‡]*School of Chemistry, Physics, and Earth Sciences, Flinders University, Adelaide, Australia 5001, and* [§]*Dipartimento di Scienze Chimiche, Università di Camerino, Via S. Agostino 1, I-62032 Camerino (MC), Italy*

antonello.filippi@uniroma1.it

Received February 25, 2009

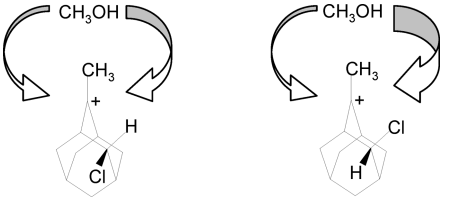

The acid-catalyzed addition of $CH_3{}^{18}OH$ to 2-methylene-adamantanes bearing a chlorine atom in the 4-*equatorial* (**1e**) or 4-*axial* (**1a**) position has been investigated in the gas phase, at 760 Torr, in the 40−120 °C temperature range. Two different experimental approaches were employed: (1) by adding neutral $CH_3{}^{18}OH$ to the 2-methyl-4-Cl-adamant-2-yl cation, generated by protonation of the corresponding 2-methylene-4-Cl-adamantane (the *extracomplex* reaction) and (2) by reaction of 2-methylene-4-Cl-adamantane with $CH_3{}^{18}OH_2{}^+$, generated by methylation of $H_2{}^{18}O$ (the *intracomplex* reaction). The crucial role of the nature of the noncovalent intermediates involved along the reaction coordinates emerges from the difference between the results obtained in the *extracomplex* and *intracomplex* reactions for both substrates investigated. The kinetic and stereochemical results indicate that the 4-Cl substituent plays a different role depending on its *equatorial* or *axial* orientation. Examination of the experimental results in the light of MP2/6-31G* theoretical calculations provides important information about the intrinsic factors governing the facial diastereoselectivity of trigonal carbocations. The effects due to differential face solvation phenomena emerge from the comparison of the present gas-phase results with those obtained from strictly related studies in solution.

Introduction

Many factors cooperate in determining the facial selectivity of trigonal carbon atoms toward a suitable reactant, including steric hindrance, conformational effects, chelation, and electronic factors, as well as temperature and nature of the solvent.[1] In recent years, the contribution of electronic factors has been the subject of intensive investigation. Most of this work dealt with the behavior of rigid model systems, i.e., neutral (**1$_{5X}$**) and charged (**I$_{5X}$**) 5-substituted adamantane derivatives, in which steric and conformational effects can be excluded (Chart 1).[2]

Although the distinct preference of nucleophilic reactants for the *syn* (*Z*) and the *anti* (*E*) face of 5-X-adamant-2-yl cations (**I$_{5X}$**) bearing, respectively, σ-electron-withdrawing (EWG) and σ-electron-donating (EDG) X substituents, is well established both in solution and in the gas phase, the origin of such behavior is not completely clear. In solution, it can be attributed to kinetic as well as thermodynamic factors, i.e., the starting relative population of the involved ions (e.g., (*E*)- (**I$^E_{5X}$**) and (*Z*)-5-X-adamant-2-yl (**I$^Z_{5X}$**)) and their interconversion rate in competition with the formation rate of the products. With a given X substituent, the relative amount of equilibrating **I$^E_{5X}$** and **I$^Z_{5X}$** cations depends on both the procedure used for generating the ions and their lifetime in the nucleophilic

[||] In honor of Prof. Ted Sorensen on the occasion of his 75th birthday.

(1) For reviews on this topic, see special issue *Chem. Rev.* **1999**, *99* (5): (a) Kaselj, M.; Chung, W.-S.; le Noble, W. J. *Chem. Rev.* **1999**, *99* (5), 1387. (b) Adcock, W.; Trout, N. A. *Chem. Rev.* **1999**, *99* (5), 1415. See also: (c) Pritt, J. R.; Whiting, M. C. *J. Chem. Soc., Perkin Trans.* **1975**, *13*, 1458 and references therein.

(2) (a) Adcock, W.; Cotton, J.; Trout, N. A. *J. Org. Chem.* **1994**, *59*, 1867. (b) Herrmann, R.; Kirmse, W. *Liebigs Ann.* **1995**, 699. (c) Adcock, W.; Head, N. J.; Lokan, N. R.; Trout, N. A. *J. Org. Chem.* **1997**, *62*, 6177. (d) Rauk, A.; Sorensen, T. S.; Schleyer, P. v. R. *J. Chem. Soc., Perkin Trans. 2* **2001**, 869.

DOI: 10.1021/jo9004298 Published on Web 06/18/2009

CHART 1

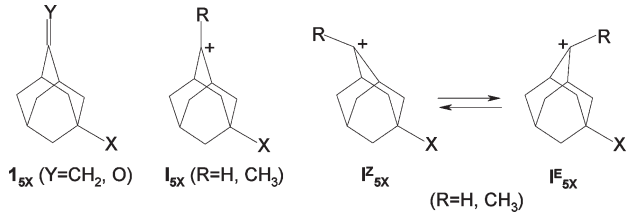

CHART 2

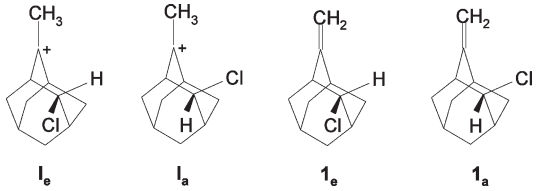

environment. In contrast, theoretical calculations indicate that, irrespective of the EDG or EWG properties of the X substituents, either a single $\mathbf{I^E_{5X}}$ or a single $\mathbf{I^Z_{5X}}$ geometry is predicted for 5-X-adamant-2-yl cations in the gas phase. Accordingly, kinetic investigations point to a gas-phase diastereoselectivity of $\mathbf{I_{5X}}$ as being mainly determined by the different space available for the incoming nucleophile toward the *syn* and the anti face of the pyramidalized $\mathbf{I^E_{5X}}$ or $\mathbf{I^Z_{5X}}$ ion. Furthermore, a comparison between the above gas-phase and solution results suggests that differential solvation effects may be important in the nucleophilic face selection process.[3]

The facial diastereoselectivity of some *equatorial* and *axial* 4-X-2-methyl-adamant-2-yl cations (X = F, Cl, Br, I) has been recently investigated in solution.[4] Here we report on the gas-phase diastereoselectivity of *equatorial* ($\mathbf{I_e}$) and *axial* ($\mathbf{I_a}$) 4-chloro-2-methyl-adamant-2-yl cations toward methanol as a nucleophile, with the hope that a comparison with solution results may contribute to a deeper knowledge of the origin of the facial selectivity of charged trigonal carbon atoms.

Results

Radiolytic Experiments. As pointed out in our previous studies on $\mathbf{I_{5X}}$ cations,[3a,3b] two radiolytic approaches can be adopted to produce the epimeric ethereal products (e.g., $\mathbf{2^E_e}$ and $\mathbf{2^Z_e}$) from a single substrate (i.e., the *equatorial* 4-chloro-2-methylene-adamantane $\mathbf{1_e}$ of Scheme 1), namely, the *extracomplex* pathway (i) or the *intracomplex* one (ii). Obviously, the same two experimental approaches produce the epimeric ethers $\mathbf{2^E_a}$ and $\mathbf{2^Z_a}$ from the *axial* 4-chloro-2-methylene-adamantane $\mathbf{1_a}$.

The *extracomplex* path (i) of Scheme 1 starts from the direct protonation of the double bond of $\mathbf{1_e}$ by the Brønsted acids $C_nH_5^+$ ($n = 1, 2$), generated by γ-radiolysis of CH_4. In principle, this process may compete with the direct protonation of the Cl atom of $\mathbf{1_e}$, which may open an additional route to products **2** (not shown in Scheme 1). Indeed, $C_nH_5^+$ ($n = 1,2$) protonation of the Cl of $\mathbf{1_e}$ would give rise to the corresponding chloronium ion, which could electrostatically coordinate the $CH_3{}^{18}OH$ molecule. Further evolution of this adduct to the σ-bonded intermediates (i.e., $\mathbf{II^Z_e}$ and $\mathbf{II^E_e}$ in Scheme 1) would influence the dynamics and the stereoselectivity of the entire process. Fortunately, such a hypothesis can be safely excluded on the grounds of the barrierless loss of HCl from Cl-protonated $\mathbf{1_e}$ (and $\mathbf{1_a}$) in the gas phase, as testified by ancillary MP2/6-31G* calculations. Therefore, ^{18}O-labeled ethers $\mathbf{2^Z_e}$ and $\mathbf{2^E_e}$ produced in the $CH_4/CH_3{}^{18}OH/\mathbf{1_e}$ mixtures (*extracomplex* path (i) in the upper part of Scheme 1) arise from *syn*/*anti* attack of $CH_3{}^{18}OH$ to $\mathbf{I_e}$ (k_{syn} and k_{anti}, respectively), followed by neutralization (k_b and k'_b, respectively) of the formed oxonium intermediates $\mathbf{II^Z_e}$ and $\mathbf{II^E_e}$ after their possible partial interconversion ($k_{Z\rightarrow E}$ and $k_{E\rightarrow Z}$).

Instead, in the $CH_3F/{}^{18}OH_2/\mathbf{1_e}$ mixtures, the ^{18}O-labeled products $\mathbf{2^Z_e}$ and $\mathbf{2^E_e}$ necessarily arise from $Me^{18}OH_2^+$ generated in situ by $(CH_3)_2F^+$-methylation of $H_2{}^{18}O$ (*intracomplex* path (ii) in the upper part of Scheme 1) and, therefore, *in the complete absence of free methanol molecules*.[3,5] Proton transfer from $Me^{18}OH_2^+$ to the double bond of $\mathbf{1_e}$ yields the $\mathbf{I_e}/Me^{18}OH$ pair, whose *intracomplex* addition yields the oxonium intermediates $\mathbf{II^Z_e}$ and $\mathbf{II^E_e}$ and, eventually, their neutral derivatives $\mathbf{2^Z_e}$ and $\mathbf{2^E_e}$. Table 1 reports the results of the *extra*- and *intracomplex* reactions on the *equatorial* $\mathbf{1_e}$ substrate. Obviously, similar patterns are valid also in the formation of $\mathbf{2^Z_a}$ and $\mathbf{2^E_a}$ from the γ-radiolysis of $CH_4/CH_3{}^{18}OH/\mathbf{1_a}$ and $CH_3F/{}^{18}OH_2/\mathbf{1_a}$ mixtures. Table 2 reports the results of the *extra*- and *intracomplex* reactions on the *axial* $\mathbf{1_a}$ substrate.

The relative yields of ethers **2** in Tables 1 and 2 are mean values from repeated experiments and have been evaluated taking into account the response factor of the detector. The ionic origin of these products was verified by the sharp decrease of their absolute yield ($G_{(M)}$) for a 5-fold increase of the concentration of the base $N(C_2H_5)_3$ in the irradiated mixtures.

Equatorial Substrate $\mathbf{1_e}$. Irrespective of the specific reaction path, whether the *extracomplex* (i) or the *intracomplex* (ii) one in Scheme 1, the relative distribution of the epimeric ethereal products $\mathbf{2^E_e}$ and $\mathbf{2^Z_e}$ reflects that of the corresponding oxonium intermediates $\mathbf{II^E_e}$ and $\mathbf{II^Z_e}$, assuming the same efficiency for their deprotonation step (k_b and k'_b in Scheme 1) by a powerful base such as $N(C_2H_5)_3$ (proton affinity (PA) = 234.7 kcal/mol).[7] The facial diastereoselectivity (k_{syn}/k_{anti}) of $\mathbf{I_e}$ toward $CH_3{}^{18}OH$ can be estimated from the measured $\mathbf{2^Z_e}/\mathbf{2^E_e}$ ratio (Table 1) once the extent of the conceivable $\mathbf{II^Z_e} \rightleftarrows \mathbf{II^E_e}$ epimerization ($k_{E\rightarrow Z}$ and $k_{Z\rightarrow E}$) before their deprotonation is taken into account. To this end, the lower part of Table 1 reveals that the *intracomplex* reaction (ii) is characterized by an almost constant distribution of the epimeric products $\mathbf{2^E_e}$ (24 ± 2%) and $\mathbf{2^Z_e}$ (76 ± 2%) within the temperature range investigated. This observation allows the formulation of two hypotheses for the behavior of their oxonium precursors $\mathbf{II^E_e}$ and $\mathbf{II^Z_e}$ from the *intracomplex* process, i.e., either they do not epimerize within their lifetime τ or if they do, they are formed in relative yields closely corresponding to their equilibrium distribution. The first hypothesis can be excluded on the grounds of ancillary experiments involving the direct O-methylation of weighed mixtures of *equatorial* 4-chloro-2-methyl-adamantan-2-ols

(3) (a) Filippi, A.; Trout, N. A.; Brunelle, P.; Adcock, W.; Sorensen, T. S.; Speranza, M. *J. Am. Chem. Soc.* **2001**, *123*, 6396–403. (b) Filippi, A.; Trout, N. A.; Brunelle, P.; Adcock, W.; Sorensen, T. S.; Speranza, M. *J. Org. Chem.* **2004**, *69*, 5537. (c) Fraschetti, C.; Novara, F. R.; Filippi, A.; Trout, N. A.; Adcock, W.; Sorensen, T. S.; Speranza, M. *J. Org. Chem.* **2007**, *72* (11), 4077.

(4) (a) Adcock, W.; Trout, N. A. *J. Phys. Org. Chem.* **2008**, *21*, 68–78. (b) Adcock, W.; Trout, N. A. *J. Phys. Org. Chem.* **2007**, *20*, 791.

(5) Blint, R. J.; McMahon, T. B.; Beauchamp, J. L. *J. Am. Chem. Soc.* **1974**, *96*, 1269.

(6) Su, T.; Chesnavitch, W. J. *J. Chem. Phys.* **1982**, *76*, 5183.

(7) Hunter, E. P.; Lias, S. G. *J. Phys. Chem. Ref. Data* **1998**, *27* (3), 413–656. http://webbook.nist.gov/chemistry/.

SCHEME 1

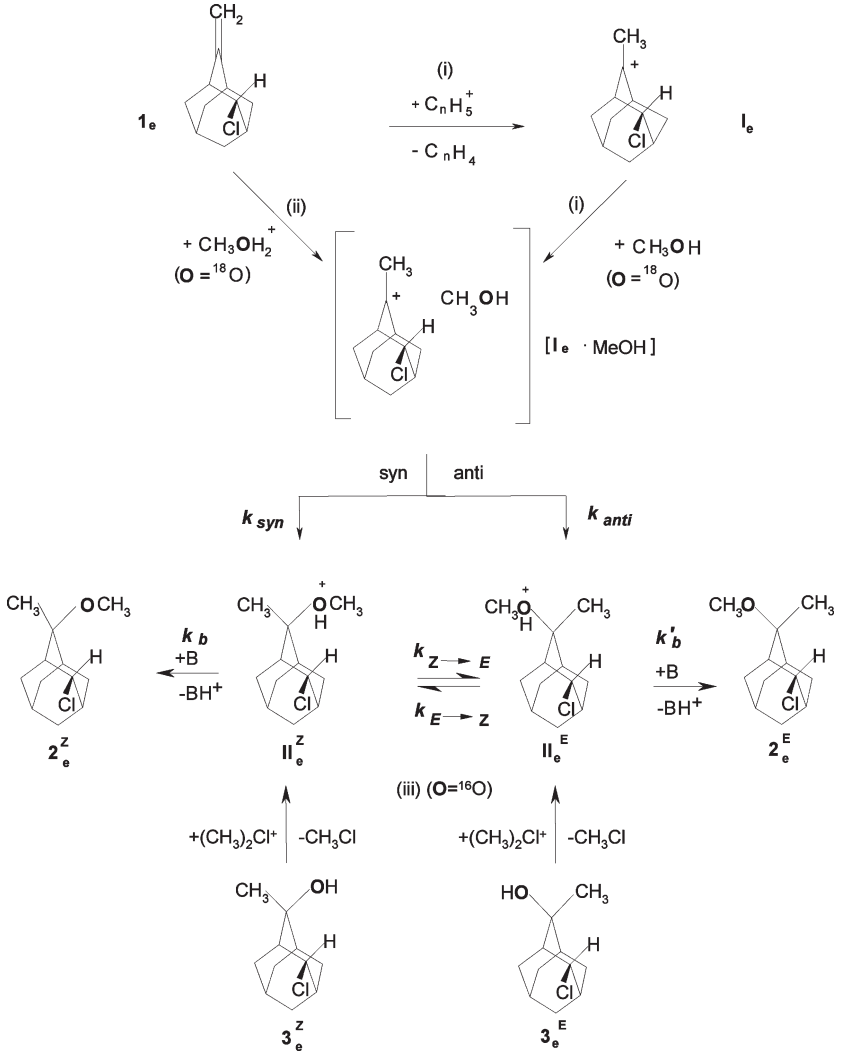

TABLE 1. Relative and Absolute Yields of ^{18}O-Labeled Ethereal Products from the Acid-Catalyzed Addition of $CH_3{}^{18}OH$ to $\mathbf{1_e}$ in the Presence of $N(C_2H_5)_3$ as a Powerful Base[a]

path[b]	T (°C)	$CH_3{}^{18}OH$ (Torr)	$N(C_2H_5)_3$ (Torr)	τ^c ($\times 10^8$ s)	$\mathbf{2^Z}_e{}^d$ (%)	$\mathbf{2^E}_e{}^d$ (%)	$G_{(M)}{}^e$ ($\times 10^2$)	$\mathbf{2^Z}_e/\mathbf{2^E}_e{}^f$
i	40	0.736	0.437	6.6	57.1	42.9	1.333	1.33 (0.124)
i	60	0.973	0.411	7.5	60.0	40.0	0.384	1.50 (0.176)
i	80	0.792	0.315	10.3	66.6	33.4	4.950	1.99 (0.299)
i	100	0.963	0.341	10.1	68.4	31.6	0.529	2.17 (0.336)
i	120	0.801	0.324	11.3	73.8	26.2	3.864	2.81 (0.449)
path[g]	T (°C)	$H_2{}^{18}O$ (Torr)	$N(C_2H_5)_3$ (Torr)	τ^c ($\times 10^8$ s)	$\mathbf{2^Z}_e{}^d$ (%)	$\mathbf{2^E}_e{}^d$ (%)	$G_{(M)}{}^e$ ($\times 10^2$)	$\mathbf{2^Z}_e/\mathbf{2^E}_e{}^f$
ii	60	3.309	0.290	10.6	78.0	22.0	0.346	3.55 (0.550)
ii	70	3.567	0.267	11.8	77.8	22.2	0.093	3.50 (0.544)
ii	80	4.691	0.339	9.6	76.7	23.3	0.488	3.29 (0.518)
ii	90	3.834	0.275	12.2	76.2	23.8	0.155	3.20 (0.506)
ii	100	3.319	0.333	10.4	75.5	24.5	0.563	3.08 (0.488)
ii	120	3.042	0.315	11.6	74.1	25.9	0.279	2.86 (0.457)

[a] Bulk gas, 750 Torr; $\mathbf{1_e}$ (0.2÷0.3 Torr); O_2 (4 Torr); radiation dose, 2×10^4 Gy (dose rate, 1×10^4 Gy h^{-1}). [b] *Extracomplex* reaction; bulk gas CH_4. [c] Reaction time calculated from the reciprocal of the first-order collision constant between intermediates $\mathbf{II^Z}_e$ and $\mathbf{II^E}_e$ and the base $N(C_2H_5)_3$.[6] [d] ^{18}O-labeled; uncertainty ca. 5%. [e] $G_{(M)}$ = number of molecules M produced per 100 eV of absorbed energy. [f] $\log(\mathbf{2^Z}_e/\mathbf{2^E}_e)$ in parentheses. [g] *Intracomplex* reaction; bulk gas CH_3F.

(i.e., $\mathbf{3^E}_e/\mathbf{3^Z}_e = 80/20$; path (iii) in Scheme 1). It is observed that the corresponding oxonium intermediates, initially formed in the $\mathbf{II^E}_e/\mathbf{II^Z}_e = 80/20$ ratio, undergo partial interconversion during their lifetime τ, as witnessed by the relative distribution of the corresponding unlabeled ethereal products $\mathbf{2^E}_e$ and $\mathbf{2^Z}_e$ (Table 3), which tends to approach the equilibrium distribution at the highest temperatures. Accordingly, the $K_{eq} = k_{Z\rightarrow E}/k_{E\rightarrow Z}$ (Scheme 1) can be roughly estimated as 0.31 from the results of the $CH_3F/H_2{}^{18}O$ mixtures (path (ii) in Table 1). Introducing this value and the $\mathbf{2^E}_e$ versus $\mathbf{2^Z}_e$ yield ratios of Table 3 into an

TABLE 2. Relative and Absolute Yields of ^{18}O-Labeled Ethereal Products from the Acid-Catalyzed Addition of $CH_3{}^{18}OH$ to $\mathbf{1_a}$ in the Presence of N$(C_2H_5)_3$ as a Powerful Base[a]

path[b]	T (°C)	$CH_3{}^{18}OH$ (Torr)	$N(C_2H_5)_3$ (Torr)	τ^c ($\times 10^8$ s)	$\mathbf{2}^{\mathbf{Z}}{}_{\mathbf{a}}{}^d$ (%)	$\mathbf{2}^{\mathbf{E}}{}_{\mathbf{a}}{}^d$ (%)	$G_{(M)}{}^e$ ($\times 10^2$)	$\mathbf{2}^{\mathbf{Z}}{}_{\mathbf{a}}/\mathbf{2}^{\mathbf{E}}{}_{\mathbf{a}}{}^f$
i	40	0.787	0.423	6.8	95.3	4.7	3.71	20.28 (1.307)
i	60	0.588	0.419	7.3	92.8	7.2	9.16	12.89 (1.110)
i	70	0.769	0.400	7.9	92.9	7.1	9.63	13.08 (1.117)
i	85	0.681	0.401	8.2	93.9	6.1	11.56	15.39 (1.187)
i	100	1.090	0.324	10.7	96.4	3.6	43.37	26.78 (1.428)
i	120	0.801	0.369	9.9	96.4	3.6	5.83	26.78 (1.428)
path[g]	T (°C)	$H_2{}^{18}O$ (Torr)	$N(C_2H_5)_3$ (Torr)	τ^c ($\times 10^8$ s)	$\mathbf{2}^{\mathbf{Z}}{}_{\mathbf{a}}{}^d$ (%)	$\mathbf{2}^{\mathbf{E}}{}_{\mathbf{a}}{}^d$ (%)	$G_{(M)}{}^e$ ($\times 10^2$)	$\mathbf{2}^{\mathbf{Z}}{}_{\mathbf{a}}/\mathbf{2}^{\mathbf{E}}{}_{\mathbf{a}}{}^f$
ii	40	3.400	0.415	6.9	42.7	57.3	0.295	0.75 (−0.128)
ii	50	4.255	0.480	6.2	53.8	46.2	0.637	1.16 (0.066)
ii	60	3.655	0.472	6.5	52.6	47.4	0.474	1.11 (0.045)
ii	70	4.003	0.542	5.8	60.8	39.2	0.859	1.55 (0.191)
ii	80	4.813	0.388	8.4	68.8	31.2	0.422	2.21 (0.343)
ii	85	3.557	0.377	8.8	66.9	33.1	1.098	2.02 (0.306)
ii	100	3.534	0.589	5.9	81.9	18.1	1.425	4.52 (0.656)
ii	110	4.780	0.613	5.8	80.9	19.1	4.506	4.24 (0.627)
ii	120	2.543	0.333	10.9	90.1	9.9	1.336	9.10 (0.959)

[a] Bulk gas, 750 Torr; $\mathbf{1_a}$ (0.2 ÷ 0.3 Torr); O_2 (4 Torr); radiation dose, 2×10^4 Gy (dose rate, 1×10^4 Gy h^{-1}). [b] *Extracomplex* reaction; bulk gas CH_4. [c] Reaction time calculated from the reciprocal of the first-order collision constant between intermediates $\mathbf{II}^{\mathbf{Z}}{}_{\mathbf{a}}$ and $\mathbf{II}^{\mathbf{E}}{}_{\mathbf{a}}$ and the base $N(C_2H_5)_3$.[6] [d] ^{18}O-labeled; uncertainty ca. 5%. [e] $G_{(M)}$ = number of molecules M produced per 100 eV of absorbed energy. [f] log($\mathbf{2}^{\mathbf{Z}}{}_{\mathbf{a}}/\mathbf{2}^{\mathbf{E}}{}_{\mathbf{a}}$) in parentheses. [g] *Intracomplex* reaction; bulk gas CH_3F.

TABLE 3. Epimerization of Ions $\mathbf{II}^{\mathbf{E}}{}_{\mathbf{e}}$ and $\mathbf{II}^{\mathbf{Z}}{}_{\mathbf{e}}$ by Gas-Phase Methylation of *E*/*Z* = 80/20 Mixtures of *Equatorial* 4-Chloro-2-methyl-adamantan-2-ol ($\mathbf{3_e}$)[a]

T (°C)	τ^b ($\times 10^8$ s)	$N(C_2H_5)_3$ (Torr)	$\mathbf{2}^{\mathbf{Z}}{}_{\mathbf{e}}{}^c$ (%)	$\mathbf{2}^{\mathbf{E}}{}_{\mathbf{e}}{}^c$ (%)	$k_{E\rightarrow Z}{}^d$ ($\times 10^{-6}$ s^{-1})	$k_{Z\rightarrow E}{}^d$ ($\times 10^{-6}$ s^{-1})
40	10.5	0.273	27.1	72.9	1.02 (6.01)	0.44 (5.64)
60	12.0	0.256	30.3	69.7	1.35 (6.13)	0.58 (5.76)
80	15.4	0.211	40.6	59.4	2.41 (6.38)	1.04 (6.02)
100	8.7	0.395	34.7	65.3	2.51 (6.40)	1.08 (6.03)
120	11.9	0.306	52.4	47.6	6.14 (6.79)	2.64 (6.42)

[a] Bulk gas, CH_3F/CH_3Cl = 10/1 (750 Torr); $\mathbf{3_e}$, 0.3−0.5 Torr; $H_2{}^{18}O$, ca. 2.5 Torr; O_2, 5 Torr; radiation dose, 2.0×10^4 Gy (dose rate, 1.0×10^4 Gy h^{-1}). [b] Reaction time calculated from the reciprocal of the first-order collision constant between intermediates $\mathbf{II}^{\mathbf{Z}}{}_{\mathbf{e}}$ and $\mathbf{II}^{\mathbf{E}}{}_{\mathbf{e}}$ and the base $N(C_2H_5)_3$.[6] [c] ^{18}O < 1%; uncertainty: ca. 5%. [d] log *k* in parentheses; assuming $K_{eq} = k_{Z\rightarrow E}/k_{E\rightarrow Z} = 0.31$ (see text).

iterative computational best-fitting program,[8] the rate constants $k_{E\rightarrow Z}$ and $k_{Z\rightarrow E}$ have been estimated (last two columns of Table 3). Linear regression analysis of these data led to the Arrhenius equations for the $\mathbf{II}^{\mathbf{Z}}{}_{\mathbf{e}} \rightarrow \mathbf{II}^{\mathbf{E}}{}_{\mathbf{e}}$ epimerization, i.e., $\log(k_{E\rightarrow Z}) = (9.5 \pm 0.6) - (5.1 \pm 0.9)1000/2.303RT$ ($r^2 = 0.908$), and for the $\mathbf{II}^{\mathbf{Z}}{}_{\mathbf{e}} \leftarrow \mathbf{II}^{\mathbf{E}}{}_{\mathbf{e}}$ one, i.e., $\log(k_{Z\rightarrow E}) = (9.1 \pm 0.6) - (5.1 \pm 0.9)1000/2.303RT$ ($r^2 = 0.907$). According to transition state theory, the activation enthalpy for both the forward and backward $\mathbf{II}^{\mathbf{Z}}{}_{\mathbf{e}} \rightleftarrows \mathbf{II}^{\mathbf{E}}{}_{\mathbf{e}}$ reactions amounts to 4.5 ± 0.6 kcal mol^{-1} and the activation entropies were -18.6 ± 3.1 and -16.9 ± 3.1 cal mol^{-1} K^{-1}, respectively. Such kinetics ($k_{E\rightarrow Z}$ and $k_{Z\rightarrow E}$) and equilibrium (K_{eq}) results allow for an estimate of the fraction of the $\mathbf{II}^{\mathbf{E}}{}_{\mathbf{e}}$ oxonium intermediate (ε), as well as that of the $\mathbf{II}^{\mathbf{Z}}{}_{\mathbf{e}}$ epimer (ζ), formed from their partial $\mathbf{II}^{\mathbf{Z}}{}_{\mathbf{e}} \rightleftarrows \mathbf{II}^{\mathbf{E}}{}_{\mathbf{e}}$ epimerization during their lifetime τ of Table 1 (eqs 1 and 2).[9]

$$\varepsilon = \varepsilon_{eq}\left[1 - \exp\left(-\frac{k_{Z\rightarrow E}\tau}{\varepsilon_{eq}}\right)\right] \quad \text{with } \varepsilon_{eq} = \frac{K_{eq}}{1 + K_{eq}} \qquad (1)$$

$$\zeta = \zeta_{eq}\left[1 - \exp\left(-\frac{k_{E\rightarrow Z}\tau}{\zeta_{eq}}\right)\right] \quad \text{with } \zeta_{eq} = \frac{1}{1 + K_{eq}} \qquad (2)$$

These values are used in eq 3 together with the measured $\mathbf{2}^{\mathbf{Z}}{}_{\mathbf{e}}$ and $\mathbf{2}^{\mathbf{E}}{}_{\mathbf{e}}$ yields of Table 1 for calculating the actual facial diastereoselectivity (k_{syn}/k_{anti}) of the *equatorial* $\mathbf{1_e}$ substrate in either the acid-catalyzed *extracomplex* (i) and *intracomplex* (ii) addition of $CH_3{}^{18}OH$.[9]

$$\frac{k_{syn}}{k_{anti}} = \frac{\mathbf{2}^{\mathbf{Z}}_{\mathbf{e}} - \zeta}{\mathbf{2}^{\mathbf{E}}_{\mathbf{e}} - \varepsilon} \qquad (3)$$

Figure 1 reports the $\log(k_{syn}/k_{anti})$ values versus $1000/2.303RT$ for the *extra-* (○) and *intracomplex* (▽) reactions on the *equatorial* ($\mathbf{1_e}$) substrate. In the same figure, the corresponding $\log(\mathbf{2}^{\mathbf{Z}}{}_{\mathbf{e}}/\mathbf{2}^{\mathbf{E}}{}_{\mathbf{e}})$ versus $1000/2.303RT$ correlations are represented by the solid symbols (●, ▼). The similarity of the straight lines obtained from regression analyses (cf. solid vs dotted lines) indicates that the epimerization contributions (ζ and ε factors for $\mathbf{II}^{\mathbf{Z}}{}_{\mathbf{e}} \rightleftarrows \mathbf{II}^{\mathbf{E}}{}_{\mathbf{e}}$) compensate each other to a considerable extent in eq 3. Figure 1 clearly shows the different facial diastereoselectivity in the *extracomplex* and *intracomplex* reactions of $\mathbf{1_e}$ in the gas phase. Accordingly, the $\log(k_{syn}/k_{anti})$ value of the *extracomplex* process increases by increasing the reaction temperature and tends to converge toward the almost *T*-independent $\log(k_{syn}/k_{anti})$ values of the *intracomplex* reaction.

The relevant differential Arrhenius equations and the corresponding thermodynamic parameters (expressed as difference between the activation parameters of the *syn* and *anti* reaction) are reported in Table 4. Accordingly, the enthalpy factors favor the *anti* attack in the *extracomplex* reaction and slightly the *syn* attack in the *intracomplex* reaction, while in both cases the entropy factors favor the *syn* attack. As a result of the combined contributions, the

(8) Integrated equation for the $\mathbf{II}^{\mathbf{Z}}{}_{\mathbf{e}} \rightleftarrows \mathbf{II}^{\mathbf{E}}{}_{\mathbf{e}}$ epimerization according to eqs 19 and 20 in Pogliani, L.; Terenzi, M. *J. Chem. Educ.* **1992**, *69*, 278.
(9) More mathematical details can be found in the appendix of ref 3a.

syn attack is always favored over the *anti* one in the temperature range investigated.

The results of theoretical calculations at the MP2/6-31G* level of theory for the *equatorial* 4-Cl system are reported in Table S1 and graphically represented in Figure 2 for the *extracomplex* and *intracomplex* processes, respectively. According to the above experimental data and within the uncertainty of the theoretical model (± 2 kcal mol^{-1}), the epimeric oxonium ions $\mathbf{II}^{\mathbf{Z}}_{\mathbf{e}}$ and $\mathbf{II}^{\mathbf{E}}_{\mathbf{e}}$ can be taken as isoenthalpic species, interconverting through an appreciable activation barrier.

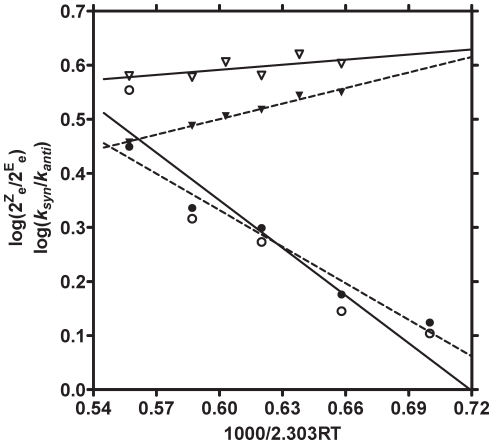

FIGURE 1. Temperature dependence of the log($\mathbf{2}^{\mathbf{Z}}_{\mathbf{e}}/\mathbf{2}^{\mathbf{E}}_{\mathbf{e}}$) from Table 1 (●, ▼ and dotted lines) and log(k_{syn}/k_{anti}) (○, ▽ and solid lines) for the *extracomplex* (circles) and *intracomplex* (triangles) acid-catalyzed addition of Me^{18}OH to $\mathbf{1}_{\mathbf{e}}$ in the gas phase.

Axial Substrate $\mathbf{1}_{\mathbf{a}}$. The methodological approaches employed for estimating the gas-phase diastereoselectivity of nucleophilic attack on *equatorial* $\mathbf{I}_{\mathbf{e}}$ can be extended to the same reactions on *axial* $\mathbf{I}_{\mathbf{a}}$. Therefore, having in mind that the 4-chloro substituent is now in the *axial* position, a labeling criterion similar to that of Scheme 1 will be used in the following discussion, the only difference being that the "**a**" (*axial*) subscript takes the place of the "**e**" (*equatorial*) one.

In the *intracomplex* reaction at 40 °C, the $\mathbf{2}^{\mathbf{E}}_{\mathbf{a}}$ product (57.3%) slightly exceeds the $\mathbf{2}^{\mathbf{Z}}_{\mathbf{a}}$ epimer (42.7%) (Table 2, Figure 3). Increasing the temperature, the product distribution tends to that observed in the *extracomplex* reaction, in which the *Z*-epimer largely dominates over the *E*-one ($\mathbf{2}^{\mathbf{E}}_{\mathbf{a}}$ (5 ± 2%) and $\mathbf{2}^{\mathbf{Z}}_{\mathbf{a}}$ (95 ± 2%); Table 2).

These raw data cannot be treated as in the previous *equatorial* case. Indeed, the $\mathbf{2}^{\mathbf{Z}}_{\mathbf{a}}/\mathbf{2}^{\mathbf{E}}_{\mathbf{a}}$ ratios measured in the *extracomplex* reaction probably are rather close to the $\mathbf{II}^{\mathbf{Z}}_{\mathbf{a}} \rightleftarrows \mathbf{II}^{\mathbf{E}}_{\mathbf{a}}$ equilibrium distribution, but in this case the small GC−MS signals of the $\mathbf{2}^{\mathbf{E}}_{\mathbf{a}}$ product are of the same order of magnitude of the uncertainty of the measure. Therefore, any conceivable temperature effect on the $\mathbf{2}^{\mathbf{Z}}_{\mathbf{a}}/\mathbf{2}^{\mathbf{E}}_{\mathbf{a}}$ distribution cannot be appreciated. Moreover, the lack of practicable synthetic routes to the $\mathbf{3}^{\mathbf{E}}_{\mathbf{a}}$ epimer prevents any reliable measurement of the extent of the conceivable $\mathbf{II}^{\mathbf{Z}}_{\mathbf{a}} \rightleftarrows \mathbf{II}^{\mathbf{E}}_{\mathbf{a}}$

TABLE 4. Differential Arrhenius Equations and Thermodynamic Parameters for the *syn* and *anti* Attack of Me^{18}OH on $\mathbf{I}_{\mathbf{e}}$ in the Gas Phase

reaction path	Arrhenius eq[a]	corr coeff, r^2	$\Delta\Delta H^{\ddagger}$[b] (kcal mol^{-1})	$\Delta\Delta S^{\ddagger}$[b] (cal mol^{-1} K^{-1})
(i) *extracomplex*	$\log(k_{syn}/k_{anti}) = (2.1 \pm 0.4) - (3.0 \pm 0.6)x$	0.880	3.0 ± 0.6	9.7 ± 2.1
(ii) *intracomplex*	$\log(k_{syn}/k_{anti}) = (0.4 \pm 0.1) + (0.3 \pm 0.2)x$	0.422	−0.3 ± 0.2	1.8 ± 0.6

[a] $x = 1000/2.303RT$. [b] $\Delta\Delta X^{\ddagger} = \Delta X^{\ddagger}_{syn} - \Delta X^{\ddagger}_{anti}$ ($X = H$, S).

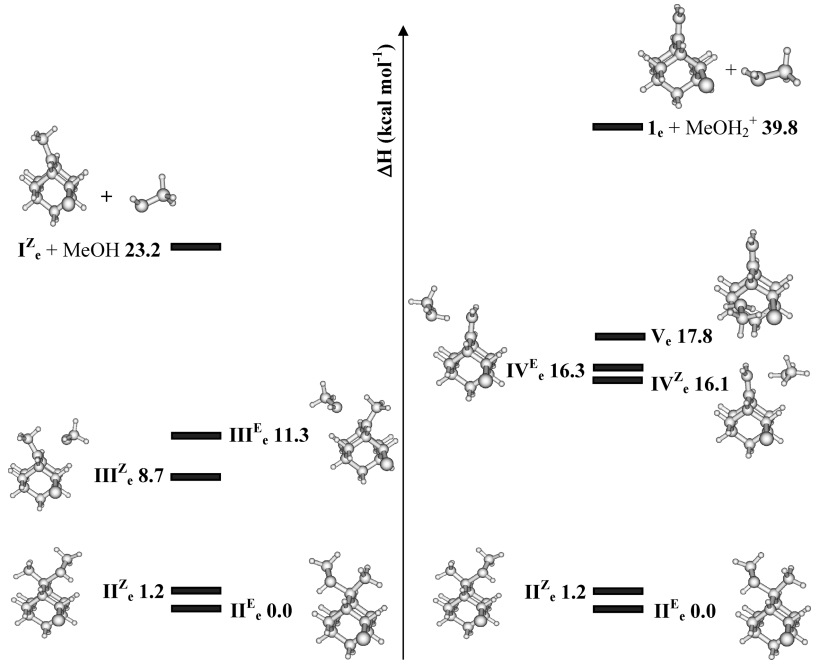

FIGURE 2. MP2/6-31G* enthalpy data (kcal mol^{-1}): (left) *equatorial* system (*extracomplex* reaction) and (right) *equatorial* system (*intracomplex* reaction) at 25 °C.

epimerization (path (iii) of Scheme 1). However, theoretical calculations (Table S2 and Figure 4) indicate that such an equilibrium ($\Delta H = 9.1$ kcal mol^{-1}) is strongly shifted to the left in full agreement with the experimental results collected in the temperature range 40−120 °C (Table 5).

Therefore, we conclude that the $\mathbf{2}^{\mathbf{Z}}_{\mathbf{a}}$ epimer is mostly formed in the *extracomplex* process ($\mathbf{2}^{\mathbf{E}}_{\mathbf{a}}$ (5 ± 2%) and $\mathbf{2}^{\mathbf{Z}}_{\mathbf{a}}$ (95 ± 2%); Table 2) and the product ratio $\mathbf{2}^{\mathbf{Z}}_{\mathbf{a}}/\mathbf{2}^{\mathbf{E}}_{\mathbf{a}} = 0.75$, measured for the *intracomplex* reaction at 40 °C, just represents an upper limit of the corresponding kinetic diastereoselectivity.

Discussion

4 Chloro-2-methyl-adamant-2-yl Cations. At the MP2/6-31G* level of theory, the structures $\mathbf{I}^{\mathbf{Z}}_{\mathbf{e}}$ and $\mathbf{I}^{\mathbf{Z}}_{\mathbf{a}}$ are calculated as the only stable forms obtained from the gas-phase protonation of the *equatorial* ($\mathbf{1}_{\mathbf{e}}$) and *axial* ($\mathbf{1}_{\mathbf{a}}$) substrates, respectively. Both of them show a pronounced pyramidal distortion at the charged C2 atom, which is pushed away from the 4-Cl-substituted face of the adamantyl cation, as depicted in Table 6.

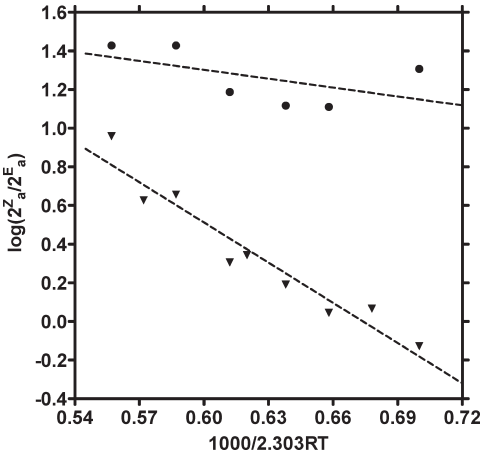

FIGURE 3. Temperature dependence of the log($\mathbf{2}^{\mathbf{Z}}_{\mathbf{a}}/\mathbf{2}^{\mathbf{E}}_{\mathbf{a}}$) from Table 2 for the *extracomplex* (●) and *intracomplex* (▼) acid-catalyzed addition of Me^{18}OH to $\mathbf{1}_{\mathbf{a}}$ in the gas phase.

Such a structural *Z*-distortion is more pronounced for the *equatorial* cation ($\theta = 17.5$, $\varphi = 6.3$) than for the *axial* analogous ($\theta = 14.8$, $\varphi = 6.0$). Several bond distances in $\mathbf{I}^{\mathbf{Z}}_{\mathbf{e}}$ and $\mathbf{I}^{\mathbf{Z}}_{\mathbf{a}}$ are also influenced by the 4-Cl atom (cf. C1−C9 and C3−C4 vs C1−C8 and C3−C10, respectively), while quite surprisingly, the same substituent does not induce any significant difference between the bond length of C3−C4 and C1−C9. At the same level of theory, a single *Z*-pyramidalized form was also found for the 5-chloro-2-methyl-adamant-2-yl cation ($\mathbf{I}^{\mathbf{Z}}_{\mathbf{5Cl}}$ in Table 6: $\theta = 17.3$, $\varphi = 6.5$). In contrast, the unsubstituted tertiary cation $\mathbf{I}_{\mathbf{H}}$ involves two fast equilibrating, resonant pyramidalized forms ($\mathbf{I}^{\mathbf{Z}}_{\mathbf{H}} \rightleftarrows \mathbf{I}^{\mathbf{E}}_{\mathbf{H}}$), whose angular distortions are calculated as $\theta = 16.9$ and $\varphi = 6.2$. Therefore, replacement of either one of the C4−H_2 or the C5−H hydrogen of $\mathbf{I}_{\mathbf{H}}$ with chlorine destabilizes the *E*-cation much more than the *Z*-cation, making the latter the only stable form at 298 K. Furthermore, since the extent of *Z*-distortion reflects the effect of the substituent to the electron demand of the charged C2 center, the above theoretical data point to a hyperconjugative effect of the chlorine atom in the remote 5 position similar to the inductive effect of the same substituent in the closer 4-*equatorial* position ($\mathbf{I}^{\mathbf{Z}}_{\mathbf{e}}$), while the same inductive effect is notably attenuated by a reversed field effect with the 4-chlorine in the *axial* position ($\mathbf{I}^{\mathbf{Z}}_{\mathbf{a}}$).[10]

Facial Diastereoselectivity of 4-Chloro-2-methyl-adamant-2-yl Cations. Figures 1 and 3 clearly show a different facial selectivity in the *extracomplex* and *intracomplex* acid-catalyzed addition of $CH_3{}^{18}OH$ to either $\mathbf{1}_{\mathbf{e}}$ and $\mathbf{1}_{\mathbf{a}}$ in the gas phase. The temperature effect is more pronounced in the

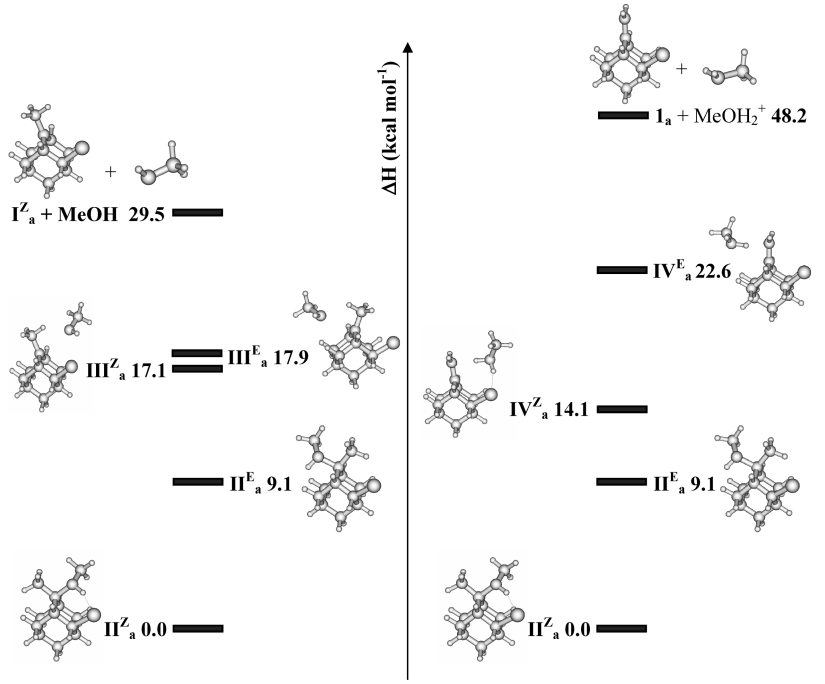

FIGURE 4. MP2/6-31G* enthalpy data (kcal mol^{-1}): (left) *axial* system (*extracomplex* reaction) and (right) *axial* system (*intracomplex* reaction) at 25 °C.

TABLE 5. Epimerization of Ions II^E_a and II^Z_a by Gas-Phase Methylation of (*Z*)-*axial* 4-Chloro-2-methyl-adamantan-2-ol (3^Z_a)[a]

T (°C)	τ^b ($\times 10^8$ s)	$N(C_2H_5)_3$ (Torr)	2^Z_e [c]	2^E_e [c]	$k_{E\rightarrow Z}$ [d] ($\times 10^{-6}$ s^{-1})	$k_{Z\rightarrow E}$ [d] ($\times 10^{-6}$ s^{-1})
40	6.8	0.423	99.9	0.1	0.26 (5.42)	0.01 (4.17)
80	8.6	0.380	99.6	0.4	0.85 (5.93)	0.05 (4.69)
100	9.6	0.360	99.4	0.6	1.17 (6.07)	0.07 (4.82)
120	11.6	0.315	99.0	1.0	1.68 (6.23)	0.10 (4.98)

[a] Bulk gas, CH_3F/CH_3Cl=10/1 (750 Torr); 3^Z_a, 0.3−0.5 Torr; $H_2{}^{18}O$, ca. 2.5 Torr; O_2, 5 Torr; radiation dose, 2.0×10^4 Gy (dose rate, 1.0×10^4 Gy h^{-1}). [b] Reaction time calculated from the reciprocal of the first-order collision constant between intermediates II^Z_a and II^E_a and the base $N(C_2H_5)_3$. [c] $^{18}O<1\%$; uncertainty: ca. 5%. [d] log k in parentheses.

TABLE 6. Calculated Geometrical Parameters of 4- and 5-Chloro-2-methyl-mdamant-2-yl Cations[a]

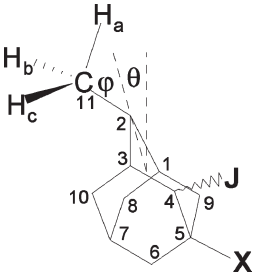

species	C1−C9 (Å)	C1−C8 (Å)	C3−C4 (Å)	C3−C10 (Å)	C2−C11 (Å)	C11−Ha (Å)	C11−Hb (Å)	C11−Hc (Å)	θ (deg)	φ (deg)
I^Z_e [b]	1.54	1.61	1.54	1.60	1.47	1.11	1.09	1.09	17.5	6.3
I^Z_a [c]	1.54	1.62	1.53	1.59	1.47	1.11	1.09	1.09	14.8	6.0
I^Z_{5Cl} [d]	1.54	1.61	1.54	1.60	1.49	1.11	1.09	1.09	17.3	6.5
I_H [e]	1.54	1.61	1.54	1.61	1.47	1.11	1.09	1.09	16.9	6.2

[a] MP2/6-31G* level of theory. [b] J = Cl_e, X = H. [c] J = Cl_a, X = H. [d] J = H, *X* = Cl. [e] X = J = H.

extracomplex than in the *intracomplex* reaction for the *equatorial* substrate, while the reverse is true for the *axial* one. At the highest temperatures, the facial diastereoselectivities of the *extracomplex* and *intracomplex* reactions converge toward a single value that is higher for the *axial* substrate than for the *equatorial* one.

The different diastereoselectivity observed in the *extracomplex* (i) and *intracomplex* (ii) reaction with $\mathbf{1_e}$ speaks against the intermediacy of the same structure for the [$\mathbf{I_e}$·MeOH] electrostatic complex (Scheme 1). The same can be said for the [$\mathbf{I_a}$·MeOH] adduct from $\mathbf{1_a}$. This means that, for both $\mathbf{1_e}$ and $\mathbf{1_a}$ substrates, paths (i) and (ii) of Scheme 1 follow different reaction coordinates.[11] The differential activation parameters of the *extracomplex* reaction on $\mathbf{1_e}$ ($\Delta\Delta H^{\ddagger} = 3.0 \pm 0.6$ kcal mol^{-1}; $\Delta\Delta S^{\ddagger} = 9.7 \pm 2.1$ cal mol^{-1} K^{-1}; Table 4) can be interpreted as follows. The pyramidal distortion of the $\mathbf{I^Z_e}$ cation (Table 6) makes its *Z*-face more accessible for the formation of the noncovalent adduct $\mathbf{III^Z_e}$ than the *E*-face for the corresponding $\mathbf{III^E_e}$ adduct (Figure 2). A similar entropy effect was found in the analogous 5-substituted cations[3a,3b] and certainly represents one of the factors favoring the *syn* selectivity of the $\mathbf{I^Z_a}$ cation (Table 6 and Figures 3 and 4). About the enthalpically favored *anti* selectivity (which contrasts with the $\mathbf{III^Z_e} > \mathbf{III^E_e}$ stability order (Figure 2)), conversion of the predominantly formed adduct $\mathbf{III^Z_e}$ to the covalent oxonium ion $\mathbf{II^Z_e}$ requires the energy-demanding breaking of the $CH_3(H)O\cdots H-CH_2-C(2)$ hydrogen bond (favored at higher temperature). In contrast, the $\mathbf{III^Z_e} \rightarrow \mathbf{II^E_e}$ conversion may take place without any pronounced hydrogen bond breaking since simple rotation of the $C(2)-CH_3$ bond brings the H-bonded nucleophile on the opposite face of the cation, just in front of the proximate C(2) center. In other words, the $\mathbf{III^Z_e} \rightarrow \mathbf{II^E_e}$ conversion does not necessarily involve the intermediacy of the loosely bound $\mathbf{III^E_e}$ adduct (whose comparatively high energy mainly arises from the cation structural distortion) but rather the intermediacy of a closely bound $\mathbf{III^Z_e}$ rotamer whose conversion to $\mathbf{II^E_e}$ involves inversion of configuration of the C(2) center energetically compensated by the incipient $CH_3(H)O\cdots C(2)$ covalent bonding.[12]

The close correspondence of the differential activation enthalpy of the *intracomplex* reaction on $\mathbf{1_e}$ ($\Delta\Delta H^{\ddagger} = -0.3 \pm 0.2$ kcal mol^{-1}; Table 4) with the computed enthalpy difference between $\mathbf{IV^E_e}$ and $\mathbf{IV^Z_e}$ adducts ($\Delta\Delta H^{\ddagger} = 0.2$ kcal mol^{-1}; Figure 2) suggests that the rate-determining steps in the reaction involve the proton transfer from $CH_3{}^{18}OH_2{}^+$ to the double bond of $\mathbf{1_e}$. Accordingly, the relatively small activation entropy difference ($\Delta\Delta S^{\ddagger} = 1.8 \pm 0.6$ cal mol^{-1} K^{-1}; Table 4) is accounted for by the almost equal probability of $CH_3{}^{18}OH_2{}^+$ attack on the *syn* and *anti* faces of $\mathbf{1_e}$. The above view conforms to the higher temperature effect observed in the *extracomplex* reaction than in the *intracomplex* one with the *equatorial* substrate.

According to Figure 4, the proton transfer between $Me^{18}OH_2{}^+$ and the *E*-face of $\mathbf{1_a}$ (via $\mathbf{IV^E_a}$: 22.6 kcal mol^{-1}) generates the $\mathbf{I_a}$ cation and the nucleophile $Me^{18}OH$, whose *intracomplex*, troposelective[13] addition favors the formation of the oxonium intermediate $\mathbf{II^E_a}$. However, when occurring

(10) Bowden, K.; Grubbs, E. J. *Chem. Soc. Rev.* **1996**, *25*, 171.
(11) Filippi, A. *Chem.—Eur. J.* **2003**, *9*, 5396.
(12) A similar feature was found for the 5-F-2-CH_3-adamant-2-yl cation, which is stable in the $\mathbf{I^Z_{5X}}$ (X = F) form in the gas phase.
(13) Filippi, A.; Speranza, M. *J. Am. Chem. Soc.* **2001**, *123*, 6077.

TABLE 7. Facial Diastereoselectivity of 4- and 5-Chloro-2-methyl-adamant-2-yl Cations at 25 °C in Gas Phase and in Solution

	$\mathbf{I_{5Cl}}$[2a,2b]		$\mathbf{I_e}$		$\mathbf{I_a}$	
	Z	*E*	*Z*	*E*	*Z*	*E*
			Gas Phase			
extracomplex[a]	75	25	52	48	95	5
intracomplex[a]	88	12	79	21	< 43	> 57
			Solvent			
CH_2Cl_2[b]	83	17	94	6	0	100
CH_3NO_2[b]	97	3	85	15		
CH_2Cl_2[c]					7	93

[a] Addition of CH_3OH; see text (Scheme 1). [b] Hydrochlorination of Cl-substituted 2-methylene-adamantane.[4b] [c] Fluorination of Cl-substituted 2-methyl-adamantan-2-ol.[4a]

on the *Z*-face of $\mathbf{1_a}$, the proton transfer involves the adduct $\mathbf{IV^Z_a}$ (Figure 4), which is stabilized (8.5 kcal mol^{-1} lower than its $\mathbf{IV^E_a}$ diastereoisomer) by the double coordination of $Me^{18}OH_2^+$ to both the unsaturated bond and the *axial* Cl atom of $\mathbf{1_a}$. It is conceivable that rearrangement of $\mathbf{IV^Z_a}$ to $\mathbf{II^Z_a}$ requires the latter interaction be weakened, a process that is favored at high temperature. It is interesting to note that the $\mathbf{2^Z_a}/\mathbf{2^E_a}$ ratio in the *intracomplex* reaction increases with the temperature and converges toward the same values of the *extracomplex* process as a consequence of the increase of the absolute yield of the $\mathbf{2^Z_a}$ product ($G_{(M)}$ column in Table 2) rather than owing to a more extended $\mathbf{II^Z_a} \rightleftarrows \mathbf{II^E_a}$ epimerization. This means that removing the $Me^{18}OH_2^+ \cdots Cl$ interaction in $\mathbf{IV^Z_a}$ favors the proton transfer to the *Z*-face of $\mathbf{1_a}$, and the behavior of the so formed $\mathbf{I_a}/Me^{18}OH$ pair becomes similar to that of the *extracomplex* process. In this view, the *axial* orientation of the 4-Cl atom heavily influences the stereochemistry of the *intracomplex* process. On the contrary, when the same substituent lies in the *equatorial* position, a similar $Me^{18}OH_2^+ \cdots Cl$ interaction yields complex $\mathbf{V_e}$ (Figure 2), which may evolve to the more stable $\mathbf{IV^Z_e}$ and $\mathbf{IV^E_e}$ adducts with almost equal probability.

Comparison with Other Gas-Phase and Solution Data. The gas-phase and solution facial diastereoselectivity of 4- and 5-chloro-substituted tertiary adamant-2-yl cations at 25 °C are reported in Table 7. Accordingly, the gas-phase acid-catalyzed addition of $CH_3{}^{18}OH$ to $\mathbf{1_a}$ is characterized by the marked preference for *syn* attack in the *extracomplex* reaction and the slight preference for *anti* product in the *intracomplex* one. Such a different diastereoselectivity reflects not only a stereoelectronic effect of the 4-Cl substituent, but also its direct involvement in the dynamics of the processes.

The exceptional *anti* selectivity shown by the same ion in solution strikingly contrasts with the observed gas-phase selectivity. Of course, such a large discrepancy cannot be entirely ascribed to a huge steric hindrance of the *axial* 4-Cl substituent toward the nucleophile in solution.[1a,4b] In previous work, the facial selectivity of various substituted 2-adamantyl cations in solution has been explained by the electronic effect of the substituent on the relative stability of rapidly equilibrating pyramidalized *E*- and *Z*-cations prior to nucleophilic capture.[14,2a,2c] Such a model is not supported by the present and previous[3a,3b] gas-phase results. Indeed, because of the exclusive occurrence of *Z*-pyramidalized 4- and 5-chloro-substituted adamant-2-yl cations in the gas phase, a much higher selectivity should be observed in the gas phase than in solution. The occurrence of the opposite trend suggests that the tertiary adamant-2-yl cations bearing EWG substituents exist as a single *Z*-pyramidalized species in both the gas phase and solution and that their facial selectivity in the latter medium may be strongly influenced by differential face solvation phenomena.

Along the same lines, the presence of the *axial* 4-Cl substituent probably induces a solvation cage denser on the *Z*-face of $\mathbf{I_a}$ than on the *E*-one, especially in close proximity to the C(2) center. Thus, relative to the *anti* attack, much more adverse desolvation extent is required in the *syn* attack of the nucleophile that may heavily contribute to the observed *anti* selectivity in solution. Obviously, the same adverse effect is absent in the gas phase and the *syn* attack via $O-H \cdots Cl$ preliminary interaction predominates. In the $\mathbf{I_e}$ analogous, the 4-Cl substituent is not able to directly induce differential face solvation phenomena, owing to its *equatorial* orientation. As a matter of fact, $\mathbf{I_e}$ shows the same *syn* selectivity in both the gas phase and solution, the latter medium being a bit more selective, as found for the 5-Cl ion $\mathbf{I_{5Cl}}$ (Table 7).

In the gas phase, the facial selectivity is more pronounced for $\mathbf{I_{5Cl}}$ than for $\mathbf{I_e}$ either in the *extracomplex* and *intracomplex* reactions at 25 °C (Table 7). According to the above discussion about the effect of the Cl-substituent on the extent of pyramidal distortion of these ions, such stereochemical results could reveal that EWG effects are transmitted more effectively from the 5- rather than the 4-position, despite the latter being closer to the C(2) center. These were also the conclusions of Grob et al.[15] based on the higher kinetic and stereochemical susceptibility to the presence of a 5- versus 4-substituent in the solvolysis of a series of adamantyl sulfonates. However, the present work, as well as our previous gas-phase investigations,[3] demonstrate that the facial selectivity depends on the combination of enthalpic and entropic effects, the latter being the dominant factor at higher temperatures. Therefore, the difference between the gas-phase face selectivity of $\mathbf{I_{5Cl}}$ and $\mathbf{I_e}$ in Table 7 cannot be directly related to the extent of transmission of electronic effects from the remote 5- or 4-positions. As a matter of fact, Grob's kinetic results correlate fairly well with inductive parameters (σ_I), but the stereochemical results are much less correlated. This is not strange if one considers that in S_N1 processes the rate determining step is not the stereoselective step, wherein other factors may play a role. Indeed, in Grob's paper the Z/E ratio is 3.33 for the 5-Cl and 0.69 for the *equatorial* 4-Cl substrate, an inversion of selectivity that cannot be simply ascribed to a different extent of Cl participation.

Conclusions

The acid-catalyzed addition of $CH_3{}^{18}OH$ to 2-methylene-adamantanes bearing a 4-chlorine atom in the *equatorial* ($\mathbf{1_e}$) or in the *axial* ($\mathbf{1_a}$) position has been investigated in the gas phase,

(14) (a) Cheung, C. K.; Tseng, L. T.; Lin, M. H.; Srivastava, S.; le Noble, W. J. *J. Am. Chem. Soc.* **1986**, *108*, 1598; 1987, *109*, 7239 . (b) Srivastava, S.; le Noble, W. J. *J. Am. Chem. Soc.* **1987**, *109*, 5874. (c) Adcock, W.; Cotton, J.; Trout, N. A. *J. Org. Chem.* **1994**, *59*, 1867. (d) Adcock, W.; Head, N. J.; Lokan, N. R.; Trout, N. A. *J. Org. Chem.* **1997**, *62*, 6177.

(15) (a) Grob, C. A.; Wittwer, G.; Rao, K. R. *Helv. Chim. Acta* **1985**, *68*, 651. (b) Grob, C. A.; Wang, G.; Wang, C. *Tetrahedron Lett.* **1987**, *28*, 1247.

at 760 Torr, in the 40−120 °C temperature range, and following two different experimental approaches (*extracomplex* and *intracomplex* reactions). The results of theoretical calculations at the MP2/6-31G* level of theory point to a single *Z*-pyramidalized tertiary cationic species ($\mathbf{I}^{\mathbf{Z}}_{\mathbf{e}}$ and $\mathbf{I}^{\mathbf{Z}}_{\mathbf{a}}$) obtained from the protonation of $\mathbf{1_e}$ and $\mathbf{1_a}$ olefins, respectively.

Both enthalpic and entropic factors account for the *syn* diastereoselectivity observed for the *extracomplex* processes of $\mathbf{1_e}$. The entropic factor is essentially related to the different space available to the incoming nucleophile on the *E* and *Z* faces of these distorted ions and the position of the transition structures along the relevant reaction coordinates. The enthalpic term is mostly related to the extent of H-bond rupture in the conversion of the primary electrostatic adducts to the covalently bonded oxonium intermediates. The *axial* orientation of the 4-Cl atom in $\mathbf{1_a}$ enables a direct involvement of the substituent in the dynamics and stereochemical outcome of the *intracomplex* reaction, favoring the *syn* product at higher temperature. A similar role is not allowed for the 4-Cl atom in $\mathbf{1_e}$ owing to its *equatorial* orientation.

The comparison of gas-phase and solution results highlights the role of differential face solvation phenomena in determining the facial stereoselectivity of trigonal carbon atoms in condensed media.

Experimental Section

Materials. Methane, methyl fluoride, and oxygen were high-purity gases and were used without further purification. $H_2{}^{18}O$ (^{18}O > 97%), $CH_3{}^{18}OH$ (^{18}O = 95%), and research grade N$(C_2H_5)_3$ were used. The *equatorial*- ($\mathbf{1_e}$) and the *axial*-4-chloro-2-methylene-adamantane ($\mathbf{1_a}$) were synthesized as described in previous papers.[4a,4b] Therein are also reported the syntheses of the $\mathbf{3^Z_e}/\mathbf{3^E_e}$ = 20/80 mixture of *equatorial* 4-chloro-2-methyl-adamantan-2-ols and of the (*Z*)-*axial* 4-chloro-2-methyl-adamantan-2-ol ($\mathbf{3^Z_a}$). Recently, we modified these procedures, increasing the product yield, but despite several attempts we were not able to obtain the (*E*)-*axial* 4-chloro-2-methyl-adamantan-2-ol ($\mathbf{3^E_a}$).[16] The methyl ethers (**2**) were prepared from the corresponding alcohols according to classical NaH/CH_3I treatment in THF under inert N_2 atmosphere at room temperature (Williamson reaction).

Radiolytic Experiments. The experimental procedure employed has been described elsewhere in detail.[3a] Briefly, 135 mL pyrex bulbs were filled up with 0.2−0.3 Torr of the substrate $\mathbf{1_e}$ or $\mathbf{1_a}$, 0.588−1.090 Torr of $CH_3{}^{18}OH$ as a nucleophile, 0.267−0.613 Torr of N$(C_2H_5)_3$ as a powerful base, 5 Torr of O_2 as an effective radical scavenger, and enough CH_4 to obtain a total pressure of about 760 Torr at the temperature of the experiment (40−120 °C). The bulbs were submitted to continuous γ-radiolysis (^{60}Co source, 1×10^4 Gy h^{-1}). Under such conditions, stationary concentrations of $C_nH_5{}^+$ (n = 1, 2) are generated and rapidly equilibrated with the gaseous dense CH_4 atmosphere before their proton transfer to the double bond of $\mathbf{1_e}$ or $\mathbf{1_a}$ to yield the corresponding 4-chloro-2-methyl-adamant-2-yl cations $\mathbf{I_e}$ or $\mathbf{I_a}$ (Scheme 1, path (i)). After collisional thermalization with the bulk gas, ions **I** react with $CH_3{}^{18}OH$ producing the oxonium intermediates $\mathbf{II^E}$ and $\mathbf{II^Z}$, whose relative amount reflects the facial diastereoselectivity (k_{syn}/k_{anti}). The final ^{18}O-labeled neutral products $\mathbf{2^E}$ and $\mathbf{2^Z}$, obtained by N$(C_2H_5)_3$ deprotonation of $\mathbf{II^E}$ and $\mathbf{II^Z}$, respectively (k'_b and k_b in Scheme 1), were analyzed by GC−MS using chiral columns (MEGADEX DACTBS-β (30% 2,3-di-*O*-acetyl-6-*O*-(*tert*-butyldimethylsilyl)-β-cyclodextrin in OV 1701, 25 m, 0.25 mm i.d., df 0.25; CHROMPACK CP-Chirasil-Dex CB, 25 m, 0.25 mm i.d., df 0.25) and authentic standard compounds for their identification. Their yields were determined from the areas of the corresponding eluted peaks, using benzyl alcohol as the internal standard and individual calibration factors to correct for the detector response. Blank experiments were carried out to exclude the occurrence of thermal decomposition and epimerization of the starting substrates, as well as the epimerization of their ethereal products within the temperature range investigated. The extent of ^{18}O incorporation into the radiolytic $\mathbf{2^E}$ and $\mathbf{2^Z}$ products and their relative yields were determined setting the quadrupole mass spectrometric detector in the selected ion mode (SIM) and analyzing the ion fragments due to CH_3 radical loss from the molecular ions (^{16}O-^{35}Cl-[M − CH_3]$^+$ at m/z = 199, ^{18}O-^{35}Cl-[M − CH_3]$^+$ and ^{16}O-^{37}Cl-[M − CH_3]$^+$ at m/z = 201, and ^{18}O-^{37}Cl-[M − CH_3]$^+$ at m/z = 203) in the relevant 70 eV electron impact (EI) spectra.

The facial diastereoselectivity of **I** ions toward methanol as a nucleophile can be inferred from the relative amount of the ethereal products $\mathbf{2^E}$ and $\mathbf{2^Z}$, once the extent of conceivable $\mathbf{II^E} \rightleftarrows \mathbf{II^Z}$ epimerization before deprotonation is assessed (ζ and ε factors in eq 3).[3a] To this end, a second set of experiments was performed under similar conditions by using the available *equatorial* or *axial* alcohols $\mathbf{3^E}/\mathbf{3^Z}$ as substrates, $H_2{}^{18}O$ as a nucleophile, and CH_3F/CH_3Cl (10/1 mixture; 760 Torr) instead of CH_4. Irradiation of these gaseous mixtures leads to the formation of stationary concentrations of $(CH_3)_2Cl^+$ ions, which act as Lewis acids by O-methylating $\mathbf{3^E}/\mathbf{3^Z}$ to give the corresponding oxonium ions (Scheme 1, path (iii)). In this way, the extent of any conceivable $\mathbf{II^E} \rightleftarrows \mathbf{II^Z}$ epimerization can be readily estimated from the relative amount of the ^{16}O neutral products $\mathbf{2^E}$ and $\mathbf{2^Z}$ measured by GC−MS as described above for the ^{18}O-labeled analogous. In this second set of experiments, $H_2{}^{18}O$ was introduced in the gaseous mixtures to check the operation of $CH_3{}^*OH_2{}^+$ ions (eventually generated by $(CH_3)_2Cl^+$ methylation of ubiquitous H_2O ($^*O{=}^{16}O$) and added $H_2{}^{18}O$ ($^*O{=}^{18}O$)) in the reaction $\mathbf{3^{E/Z}} + CH_3{}^*OH_2{}^+ \rightarrow {}^*\mathbf{II^{E/Z}} + H_2O$ as an alternative to path (iii) in Scheme 1 to products $\mathbf{2^E}$ and $\mathbf{2^Z}$.[17]

Finally, *equatorial* ($\mathbf{1_e}$) and *axial* ($\mathbf{1_a}$) substrates mixed with $H_2{}^{18}O$ (2.543−4.813 Torr), O_2 and N$(C_2H_5)_3$ as above, and CH_3F (up to 760 Torr) were submitted to γ-radiolysis with the aim of investigating the facial selectivity in the *intracomplex*[3a,3b] process $\mathbf{1} + CH_3{}^{18}OH_2{}^+ \rightarrow \mathbf{II^{E/Z}}$ (path (ii) in Scheme 1), in which $CH_3{}^{18}OH_2{}^+$ is produced in situ by $(CH_3)_2F^+$ methylation of $H_2{}^{18}O$.[17]

Computational Details. Theoretical calculations were carried out using the Gaussian 03 suite of programs[18] installed on dual processor Opteron workstations. The calculations were carried out at the MP2/6-31G*[19] level of theory. Trial input geometries for *E*- and *Z*-epimeric $\mathbf{I_e}$ and $\mathbf{I_a}$ ions were constructed based on the facially selective C−C hyperconjugation model previously

(16) Barboni, L.; Giuli, S.; Filippi, A.; Fraschetti, C.; Marcolini, M.; Marcantoni, E. *Tetrahedron. Lett.* **2008**, *49*, 6065.

(17) Contrary to $(CH_3)_2F^+$, $(CH_3)_2Cl^+$ is almost unable to methylate H_2O. See also ref 3a, 3b and references therein.

(18) Frisch, M. J.; Trucks, G. W.; Schlegel, H. B.; Scuseria, G. E.; Robb, M. A.; Cheeseman, J. R.; . Montgomery, J. A., Jr.; Vreven, T.; Kudin, K. N.; Burant, J. C.; Millam, J. M.; Iyengar, S. S.; Tomasi, J.; Barone, V.; Mennucci, B.; Cossi, M.; Scalmani, G.; Rega, N.; Petersson, G. A.; Nakatsuji, H.; Hada, M.; Ehara, M.; Toyota, K.; Fukuda, R.; Hasegawa, J.; Ishida, M.; Nakajima, T.; Honda, Y.; Kitao, O.; Nakai, H.; Klene, M.; Li, X.; Knox, J. E.; Hratchian, H. P.; Cross, J. B.; Adamo, C.; Jaramillo, J.; Gomperts, R.; Stratmann, R. E.; Yazyev, O.; Austin, A. J.; Cammi, R.; Pomelli, C.; Ochterski, J. W.; Ayala, P. Y.; Morokuma, K.; Voth, G. A.; Salvador, P.; Dannenberg, J. J.; Zakrzewski, V. G.; Dapprich, S.; Daniels, A. D.; Strain, M. C.; Farkas, O.; Malick, D. K.; Rabuck, A. D.; Raghavachari, K.; Foresman, J. B.; Ortiz, J. V.; Cui, Q.; Baboul, A. G.; Clifford, S.; Cioslowski, J.; Stefanov, B. B.; Liu, G.; Liashenko, A.; Piskorz, P.; Komaromi, I.; Martin, R. L.; Fox, D. J.; Keith, T.; Al-Laham, M. A.; Peng, C. Y.; Nanayakkara, A.; Challacombe, M.; Gill, P. M. W.; Johnson, B.; Chen, W.; Wong, M. W.; Gonzalez, C.; Pople, J. A. *Gaussian 03, Revision C.02*; Gaussian, Inc.: Wallingford, CT, 2004.

(19) Møller, C.; Plesset, M. S. *Phys. Rev.* **1934**, *46*, 618.

found for the parent 2-adamantyl cation.[20] At the same level of theory, frequency calculations were performed for all the critical point located to ascertain their minimum or transition state nature. Thermal contribution to enthalpy at 298 K and 1 atm, which include the effects of translation, rotation, and vibration, was evaluated by classical statistical thermodynamics within the approximation of ideal gas, rigid rotor, and harmonic oscillator behavior and using the recommended scaling factor for frequencies and zero point energy corrections.[21]

(20) Dutler R.; Rauk A.; Sorensen T. S.; Whitworth S. M. *J. Am. Chem. Soc.* **1989**, *111*, 9024 and references therein.
(21) Scott, A. P.; Radom, L. *J. Phys. Chem.* **1996**, *100*, 16502.

Acknowledgment. Work supported by the Australian Research Council and the Ministero dell'Istruzione dell'Università e della Ricerca (MiUR). Financial supports by Università "Sapienza", Roma, Italy (PRIN grant 2007H9S8SW_002) are acknowledged. Ms. Valentina Lilla is acknowledged for helpful technical contribution.

Supporting Information Available: MP2/6-31G* optimized geometrical parameters and relevant thermochemical data for all the calculated structures reported in Figures 2 and 4. This material is available free of charge via the Internet at http://pubs.acs.org.